Open access • Journal Article • DOI:10.1021/ACS.JOC.9B00389

Bis-4-aza[6]helicene: A Bis-helicenic 2,2'-Bipyridine with Chemically Triggered Chiroptical Switching Activity. — Source link

Helena Isla, Nidal Saleh, Jiang-Kun Ou-Yang, Kais Dhbaibi ...+8 more authors

Institutions: University of Rennes, University of Gabès, Aix-Marseille University, Jagiellonian University

Published on: 29 Mar 2019 - Journal of Organic Chemistry (American Chemical Society)

Topics: Bipyridine, 2,2'-Bipyridine, Protonation, Negishi coupling and Deprotonation

Bis-4-aza[6]helicene: a bis-helicenic 2,2'-bipyridine with chemically-triggered chiroptical switching activity

Helena Isla, Nidal Saleh, Jiang-Kun Ou-Yang, Kais Dhbaibi, Marion Jean, Magdalena Dziurka, Ludovic Favereau, Nicolas Vanthuyne, Loic Toupet, Bassem Jamoussi, et al.

Bis-4-aza[6]helicene: a bis-helicenic 2,2'-bipyridine with chemically-triggered chiroptical switching activity

Helena Isla,[†] Nidal Saleh,[†] Jiang-Kun Ou-Yang,[†] Kais Dhbaibi,[†,&] Marion Jean,[‡] Magdalena Dziurka,[#] Ludovic Favereau,[†] Nicolas Vanthuyne,[‡] Loïc Toupet,[†] Bassem Jamoussi,[&,¶] Monika Srebro-Hooper,*[,#] Jeanne Crassous*[,†]

[†] Univ Rennes, Institut des Sciences Chimiques de Rennes, UMR CNRS 6226 Campus de Beaulieu, 35042, Rennes Cedex, France. [&] University of Gabès, Faculty of Science of Gabès, Zrig, 6072 Gabès, Tunisia. [‡] Aix Marseille Université, CNRS, Centrale Marseille, iSm2, Marseille, France. [¶] Université Virtuelle de Tunis, UR17ES01 Didactique des Sciences Expérimentales et de Chimie Supramoléculaire, Tunis, Tunisia. [#] Faculty of Chemistry, Jagiellonian University, Gronostajowa 2, 30-387 Krakow, Poland.

RECEIVED DATE (will be automatically inserted after manuscript is accepted).

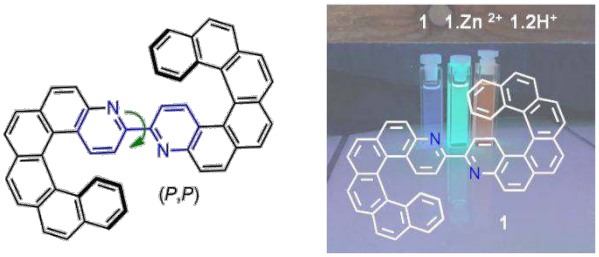

ABSTRACT. A novel enantiopure bis-helicenic 2,2'-bipyridine system was prepared using a Negishi coupling. Thanks to the bipyridine unit, the coordination with Zn^{II} and protonation processes were studied revealing efficient tuning of photophysical (UV/Visible and emission) and chiroptical properties (electronic circular dichroism and circularly polarized emission) of the system. The coordination/decoordination and protonation/deprotonation processes appeared reversible thus constituting novel chiroptical switches.

INTRODUCTION

Chirality, ubiquitous in life and in chemical substances, has growing implications in diverse domains of materials science.[1] Indeed, there is a great demand in the development of novel chiral molecules and architectures with tunable electronic and optical properties, which may be used in molecular functional devices. In particular, contributions to the field of chiroptical switches[2] are stimulated by their potential applications as molecular memory elements or logic operators, in which data storage and processing are the ultimate goals.[3] Chiroptical switches have also found applications in sensing, especially in the detection of a multitude of different chiral analytes with a high level of sensitivity,[4] in asymmetric catalysis to offer switchable stereoselectivity,[5] and in molecular motors since chirality can provide unidirectionality, an important aspect in rotatory motors such as in the biological case of ATP-synthase and other original kinds of motions.[2,3] Among chiroptical switching materials, helicenes play an increasing role due to their unprecedented inherent helical chirality accompanied by a π-conjugated electronic structure.[6] The most appealing attributes of helicene derivatives are their large-magnitude chiroptical properties, *i.e.* optical rotation (OR), electronic circular dichroism (ECD), vibrational circular dichroism (VCD), and circularly polarized luminescence (CPL).[7]

Despite remarkable progress that has been accomplished in helicene chemistry in the last decade, the development of straightforward and efficient strategies to diversify helicenes structure still remains a challenge for synthetic chemists. An attractive alternative to a stepwise organic approach to a construction of complex helicene-based architectures is coordination chemistry.[8,9] Indeed, metals are powerful templates for assembling π-conjugated ligands into well-defined molecular structures.[10] Furthermore, as the nature of the metal can strongly impact the chiroptical properties of the helical molecules, such connections give rise to chiral molecular systems combining novel topological features with enhanced photophysical and optical properties. In particular, one can take benefit from the inherent properties of a ligand and a metal ion to easily access novel helicene-based organometallic chiroptical switches[6e,f] through the action of different stimuli such as a redox potential[10a-f] or chemicals.[10g,h,11] In addition, the coordination process can induce strong conformational changes and intramolecular motions based on which new chiral switches and molecular motors can be envisioned.[11]

Among the helicenes bearing heteroatoms, azahelicenes[12] are especially interesting due to possibilities that nitrogen atoms offer. The involvement of the N lone-pair in coordination or protonation processes can induce a peculiar impact on the chiroptical properties of the helicene molecule. The bipyridine core, with the most widely used 2,2'-bipyridine unit[13] (Scheme 1), has received much attention due to its remarkable stability and exceptional coordination chemistry. Functionalized helical bipyridine systems[10d,h,13,14] exhibit an appealing set of properties: chirality, an extended π-electron system, rich and high-affinity coordination chemistry with metals, good acid/base and alkylation reactivity, and redox activity. Complexation of such systems with a metallic ion (e.g. Zn^{II}, Ru^{II}, Os^{II}, Re^{I}) may enhance their properties even further, based on strong optical activity, emission properties, and redox activity furnished by the metal. All this makes helicenic-bipyridines promising candidates for unprecedented chiroptical switches.

In this article, we present the synthesis of a bis-azahelicenic system in which bipyridine core is integrated in the sophisticated aza[6]helicene structure (**1**, Scheme 1), and we address its chiroptical switching activity triggered chemically by (*i*) Zn^{II} coordination/decoordination, and (*ii*) protonation/deprotonation processes. Read-out signals are observed using UV/Vis, ECD, OR, and luminescence techniques, and interpreted on the basis of first-principle calculations. As complexation/decomplexation process induces large conformational changes and therefore molecular motions around the zinc center, reversibly interconverting transoid and cisoid forms of **1** with different relative orientations of helicenes moieties, we also explore computationally

unidirectionality of the motion and a possible application of **1** as a molecular hinge.

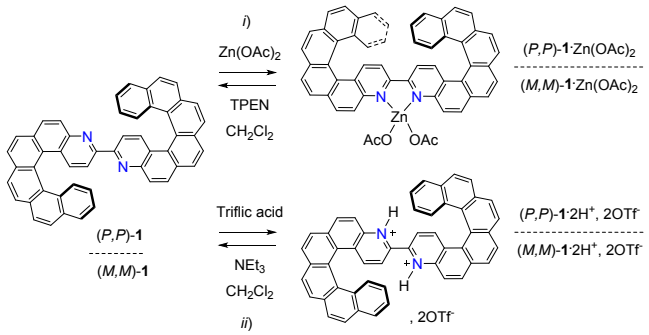

Scheme 1. Chemical structure of the bis-helicenic 2,2'-bipyridine **1** and reversible (*i*) coordination/decoordination process using $Zn(OAc)_2$/TPEN chemical stimuli and (*ii*) protonation/deprotonation with triflic acid/NEt_3 as acid/base agents in dichloromethane.

RESULTS AND DISCUSSION

Synthesis and characterization of bis-helicene-bipyridine 1.

The synthetic strategy chosen for the construction of the helical architectures **1** is based on the Negishi coupling[15] between the bromoaza[6]helicene **5** with the zinc bromide derivative **6** (see Scheme 2). The 3-bromo-4-aza[6]helicene **5** was first prepared in two steps involving a Wittig reaction between 2-methyl-naphthalene-phosphonium bromide **2**[16] and commercially available 2-bromo-pyridine-6-carboxaldehyde **3**, yielding olefin **4** as a mixture of *cis* and *trans* isomers, followed by a photocyclization reaction with a 150 W mercury lamp with 2 equiv. of iodine and an excess of propylene oxide in toluene for 15 hrs. It is worth noting that the photo-irradiation conditions were compatible with the bromo-substituent functionality. Compound **5** was obtained in the racemic form and fully characterized by NMR spectroscopy and mass spectrometry (see Supporting Information, SI). For example, it displayed two unresolved triplets around 6.8 and 7.3 ppm that are typical of protons H^{15} and H^{14}, respectively.[11b] Its structure was further ascertained by X-ray crystallographic analysis (see Figure 1 and SI). Racemic **5** crystallized in the *P*-1 space group. It displayed a helicity (dihedral angle between the two terminal rings) of 49.71° and a C-Br bond length of 1.917 Å which both correspond to regular values. Compound **5** can further be obtained as enantiopure *P*-(+)- and *M*-(-) samples by HPLC separation over a chiral stationary phase (see SI).

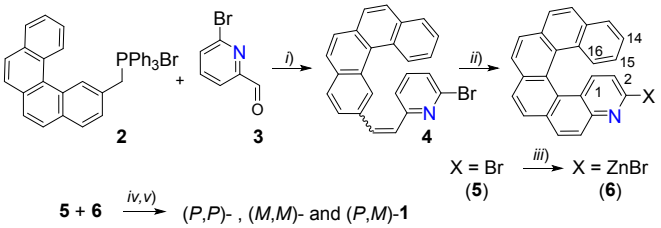

Scheme 2. Synthesis of **1** as a mixture of (*P*,*P*), (*M*,*M*), and (*P*,*M*) stereoisomers. *i*) *n*-BuLi, THF, rt, Ar, 5 hrs, 90%; *ii*) hν, I_2 (2 equiv.), propylene oxide (49 equivs), toluene, rt, Ar, 15 hrs, 45%; *iii*) *n*-BuLi, $ZnCl_2$, THF, rt, Ar, 5 hrs, 90%; *iv*) $Pd(PPh_3)_4$, THF, reflux, Ar, 15 hrs; *v*) TPEN, CH_2Cl_2, 57% (two steps).

The bis-helicenic bipyridine system **1** was prepared by generating *in situ* the zinc bromide derivative **6** from **5** followed by coupling **5** and **6** together under the regular Negishi coupling conditions. Finally, decoordination of the Zn using an excess of *N*,*N*,*N*',*N*'-tetrakis(2-pyridylmethyl)ethane-1,2-diamine (TPEN) was necessary to obtain pure **1** with 57% yield. Under these conditions and starting from racemic (±)-**5**, a mixture of stereoisomers, namely chiral (*P*,*P*)- and (*M*,*M*)-**1** and achiral *meso* compound (*P*,*M*)-**1** was expected. This was indeed evidenced by chiral HPLC analysis, which showed three peaks in 34:34:24 respective proportions (see SI).

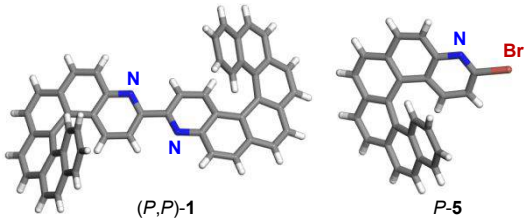

Figure 1. X-ray crystallographic structures of compounds **1** and **5** (only one stereoisomer is shown).

Single crystals of (±)-**1** were grown from pentane diffusion into a dichloromethane solution. X-ray crystallography revealed a mixture of (*P*,*P*)- and (*M*,*M*)-**1** (*P*ccn orthorhombic centrosymmetric space group, see Figure 1 and SI). The structure showed *i*) the C_1 symmetry of the chiral compound **1**, *ii*) the two nitrogen atoms placed *trans* to one another as common for 2,2'-bipyridines[13] with a dihedral angle between the different pyridine rings lower than 20°, and *iii*) typical helicity value of the azahelicene moieties (59.83°).[12] Compound (*P**,*P**)-**1**[17] was also characterized by NMR spectroscopy. For example, its ^1H NMR spectrum displayed the two typical unresolved triplets around 6.9 and 7.4 ppm corresponding to protons H^{15} and H^{14}, respectively. Note that the low quantities isolated and solubility issues did not allow to characterize the *meso*-**1** compound by NMR spectroscopy. However, sufficient amounts of enantiopure (*P*,*P*)- and (*M*,*M*)-**1** compounds were directly prepared under similar Negishi coupling conditions from enantiopure *P*- and *M*-**5** samples.

Photophysical and chiroptical properties of (*P*,*P*)- and (*M*,*M*)-1

Photophysical and chiroptical properties of **1** were then examined and compared to those of the precursor **5**. As seen in Figure 2a, the UV/Visible spectrum of (*P**,*P**)-**1**[17] shows a very strong absorption band centered around 275 nm ($\varepsilon \sim 7.6 \times 10^4$ M^{-1} cm^{-1}) and a set of bands of gradually diminishing intensity that extends into the visible region with the longest absorption wavelength appearing at 420 nm ($\varepsilon \sim 10^4$ M^{-1} cm^{-1}). In comparison, the compound **5** displays overall less intense UV/Vis bands with the stronger one at 262 nm ($\varepsilon \sim 5.7 \times 10^4$ M^{-1} cm^{-1}) and the weaker one at the longest wavelength of 405 nm ($\varepsilon \sim 10^3$ M^{-1} cm^{-1}). Furthermore, while **5** is not emissive, likely due to fluorescence quenching via internal heavy atom (Br) effect,[18] (*P**,*P**)-**1**[17] displays rather intense blue fluorescence in CH_2Cl_2 at rt (λ_{max} = 420 nm, ϕ = 22%, Table S1.1 in the SI, and Figure 4c). Its structured emission spectrum is characterized by a vibronic progression of ~ 1350 cm^{-1} with the maximum intensity being in the 0-0 band

that is indicative of a rigid aromatic fluorophore. Note that emission behavior of **1** is almost identical to that previously observed for helicenic bipyridine and terpyridine systems.[10h,11] Linear-response time-dependent density functional theory (TDDFT) calculations,[19] following the computational protocol that was established in Ref. 11 for a bis-helicenic terpyridine ligand and a corresponding Zn-based complex, reproduce experimental data well (see Figure 2a, inset, and Table S2.9 in the SI). Details regarding all the calculations presented in this article along with additional results not discussed herein in detail are provided in the SI. As expected, enhanced UV/Vis properties of **1** as compared to **5** can be linked to its extended π-conjugation involving both azahelicene fragments. Indeed, the additional low-energy (> 350 nm) absorption observed for **1** originates from excitations (nos. 1 calculated at 372 nm and 3 at 359 nm) that may be predominantly considered as π-π* transitions across the whole molecule with some charge transfer (CT) components from helicene moieties to bipyridine fragment due to a partial spatial separation of the engaged MOs. For example, both excitations demonstrate high HOMO-LUMO contributions, with HOMO almost evenly extended over π-electron system within the whole molecule and LUMO localized predominantly onto bipyridine fragment and its adjacent helicene rings (see Figure 3). The same was found for the frontier MOs at the optimized S_1 excited-state geometry that supports a predominantly bipyridine-centered LUMO-HOMO emission for **1**.

Intense mirror-image ECD spectra were then recorded for (*M*,*M*)- and (*P*,*P*)-**1** enantiomers (Figure 2b), showing a strong negative band around 273 nm ($\Delta\varepsilon$ = -333 M^{-1} cm^{-1}) and strong positive one at 332 nm ($\Delta\varepsilon$ = +309 M^{-1} cm^{-1}) for the (*P*,*P*)-**1**. Weaker positive ECD bands are also present at longer wavelengths between 380 and 420 nm, *i.e.* at 382 ($\Delta\varepsilon$ = +70 M^{-1} cm^{-1}), 397 ($\Delta\varepsilon$ = +26 M^{-1} cm^{-1}) and 417 nm ($\Delta\varepsilon$ = +23 M^{-1} cm^{-1}). For comparison, the *P*-**5** displays a weaker ECD spectrum than (*P*,*P*)-**1** and similar to those observed for other carbo[6]helicene derivatives, with a strong negative band around 258 nm ($\Delta\varepsilon$ = -200 M^{-1} cm^{-1}), a strong positive one at 326 ($\Delta\varepsilon$ = +173 M^{-1} cm^{-1}), and no ECD-active band above 380 nm. Note that some vibronic structure is roughly seen in both compounds **1** and **5**. As seen in Figure 2b, inset, the calculated ECD spectral features of **1** and **5** agree well with the experiment. The MO analysis of dominant excitations calculated in the low- and medium-energy regions of the simulated ECD spectra of (*P*,*P*)-**1** confirms that its main highly intense positive band originates predominantly from π-π* transitions within helicene moieties accompanied by helicene→bipyridine and bipyridine→helicene CTs. See for example, excitations nos. 2, 5, and 6 with sizable rotatory strengths calculated at respectively 368, 331, and 322 nm and their MO assignment in the SI. This clearly highlights the effect of elongated π-electron system due to the presence of two azahelicene moieties in **1**, resulting in a strong enhancement of its chiroptical properties as compared to **5**. In line with the ECD spectra, high specific and molar optical rotation values were thus obtained for **1** with its molar rotation 1.7 times higher than for **5** ((*P*,*P*)-**1**: $[\alpha]_D^{23}$ = +2600° cm^2 g^{-1}, $[\phi]_D^{23}$ = +17300° cm^2 $dmol^{-1}$ (±5%, CH_2Cl_2, 4.2 × 10^{-5} M) vs. *P*-**5**: $[\alpha]_D^{23}$ = +2500° cm^2 g^{-1}, $[\phi]_D^{23}$ = +10200° cm^2 $dmol^{-1}$ (±5%, CH_2Cl_2, 6 × 10^{-6} M).

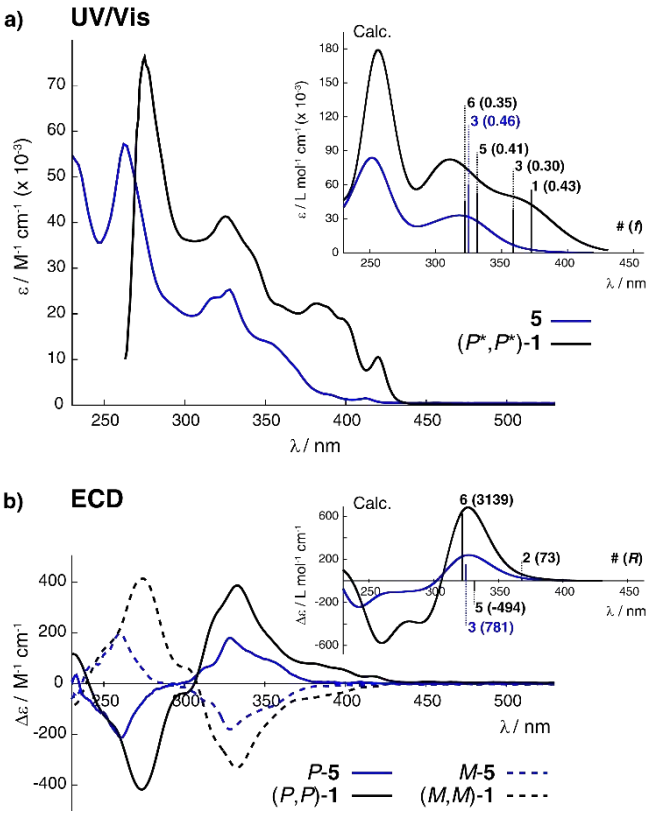

Figure 2. Experimental UV/Vis spectra of **5** and (*P**,*P**)-**1**[17] (panel a) and ECD spectra of enantiopure *M*- and *P*-**5** and (*M*,*M*)- and (*P*,*P*)-**1** (panel b) in CH_2Cl_2 ($C \sim 3 \times 10^{-5}$ M). Insets: Corresponding TDDFT (LC-PBE0*/SV(P) with a continuum solvent model for CH_2Cl_2) calculated data. No spectral shift has been applied. Numbered excitations (with oscillator strength *f*, and rotatory strength *R*, in 10^{-40} cgs, values given in parentheses) are those analyzed in detail. See also SI.

Coordination-induced chiroptical switching activity and molecular motion in bis-helicenic bipyridine 1

The bipyridine system is a good scaffold for coordination to a variety of transition-metal centers yielding complexes with diversity of photophysical properties that may be appealing for device applications.[13] For example, Rebek, Jr. et al. have integrated crown ether functionalities within the 2,2'-bipyridine platform to study allosteric effects.[20] Furthermore, the molecular engineering of 2,2'-bipyridines with chiral units, introducing controlled steric congestion and chirality, enables to construct fascinating helicate structures,[21a] and molecular motors displaying unidirectionality. Indeed, regarding the latter property, Haberhauer has designed a molecular hinge based on a 2,2'-bipyridine derivative grafted with a chiral peptidic clamp that shows a unidirectional open-close motion upon coordination to a Cu^{II} chemical stimulus.[21b,c] Yashima and co-workers have developed unprecedented molecular springs consisting of enantiomeric double-stranded spiroborate helicates bearing 2,2'-bipyridine and its N,N-dioxide linkages that demonstrate a unique allosterically regulated reversible extension-contraction motions coupled with unidirectional and helicity conservative twisting upon binding or release of protons and/or metal ions.[21d]

These examples open up the possibility for further design and development of molecular machines, both simpler or even more sophisticated ones. Based on this idea, we then explored how Zn^{II} binding to a bis-helicenic 2,2'-bipyridine system could induce chemical switching of the UV/Vis absorption, ECD, and luminescence spectra via addition of *i*) $Zn(OAc)_2$ for coordination and *ii*) TPEN for decoordination (see Scheme 1).

Aliquots of $Zn(OAc)_2 \cdot 2H_2O$ (0.2 equiv. until saturation at 1.0-1.2 equivs) were thus added to **1** and the complexation process was followed by UV/Vis, ECD, and emission spectroscopy (Figure 4a-c). Several changes were observed in the UV/Vis spectrum of (*P**,*P**)-**1**[17] upon Zn^{II} binding, as depicted in Figure 4a, with the presence of several isosbestic points, showing that the two species are in exchange. The main modification of the spectrum appears between 420 and 500 nm where an additional band emerges upon Zn complexation. Accordingly, a colour of the solution turned from pale yellow to dark yellow. Substantial modifications were also observed for chiroptical properties of (*M*,*M*)-**1** after

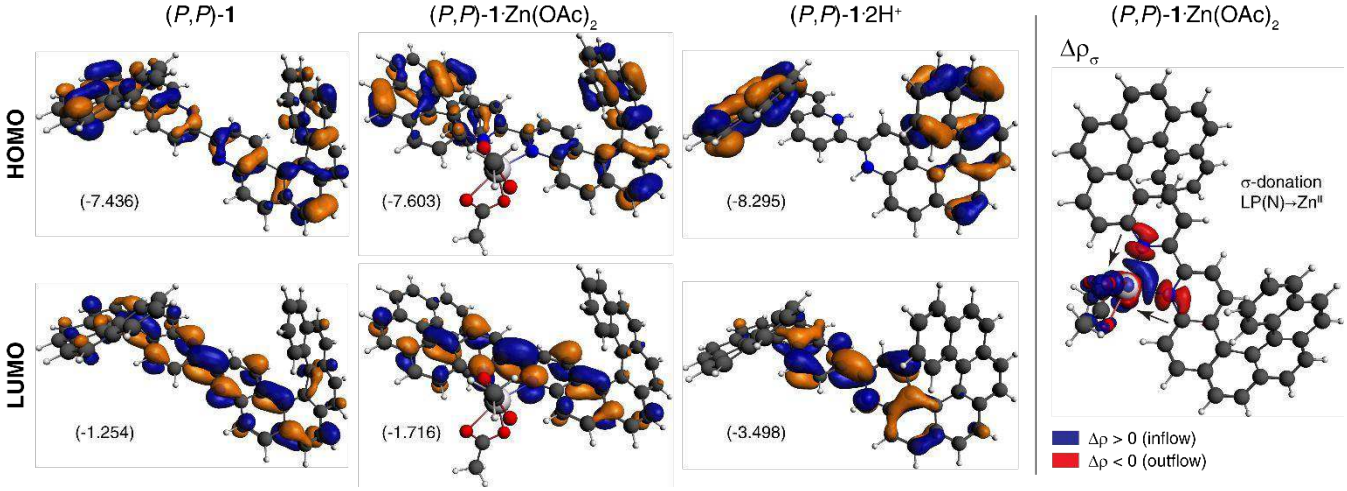

Figure 3. Left: Isosurfaces (±0.03 au) of frontier MOs of the bis-helicenic bipyridine ligand **1**, of its corresponding Zn complex **1**·$Zn(OAc)_2$, and of its doubly protonated species **1**·$2H^+$. Right: Isosurface (±0.0015 au) of dominant ETS-NOCV deformation density channel depicting formation of the **1**–$Zn(OAc)_2$ bonding. Only the most populated (lowest-energy) conformers' results have been shown; see SI for a full set of data.

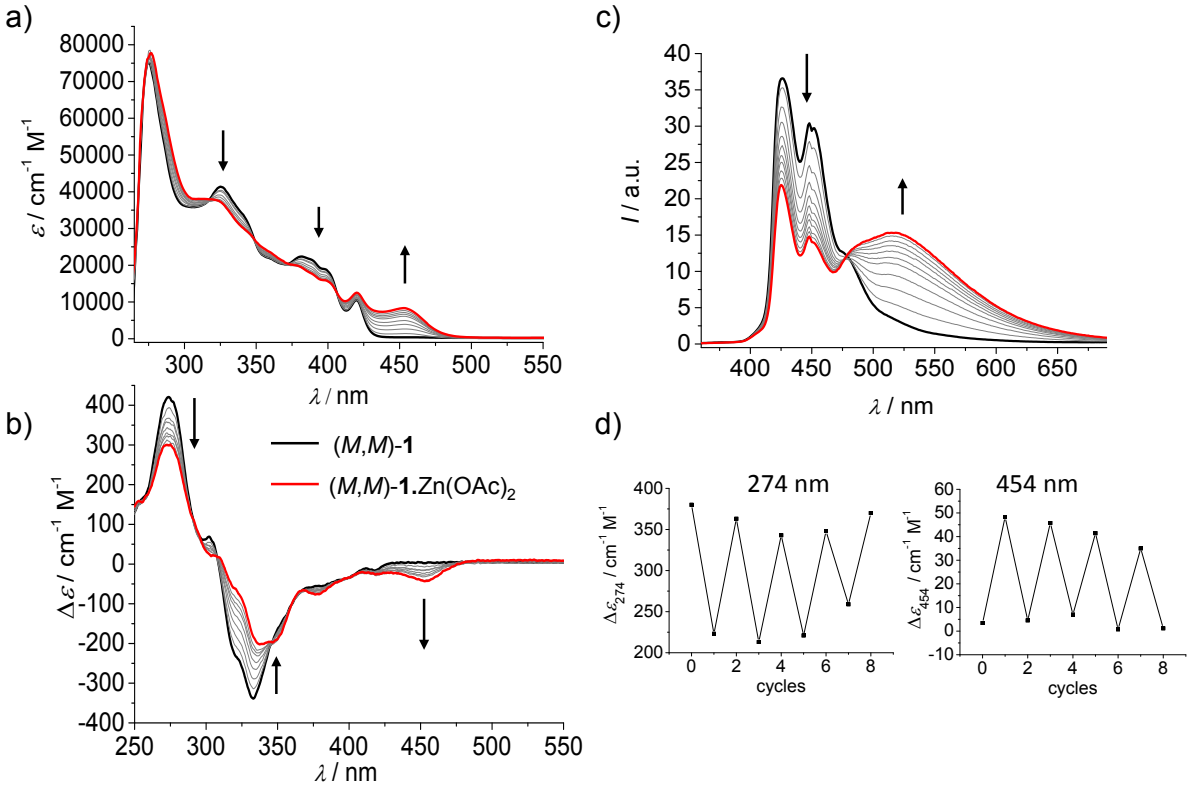

Figure 4. Evolution of UV/Vis spectrum of (*P**,*P**)-**1**[17] (panel a) and ECD spectrum of (*M*,*M*)-**1** (panel b) upon addition of $Zn(OAc)_2 \cdot 2H_2O$ aliquots (0.2 equiv. until saturation at 1.0-1.2 equivs; *C* 3×10^{-5} M, CH_2Cl_2, rt). Panel c: Evolution of fluorescence of (*P**,*P**)-**1**[17] ($\lambda_{ex} = 350$ nm, *C* 2.2×10^{-5} M, CH_2Cl_2, rt). Panel d: Reversible ECD_{274nm} and ECD_{454nm} switching process.

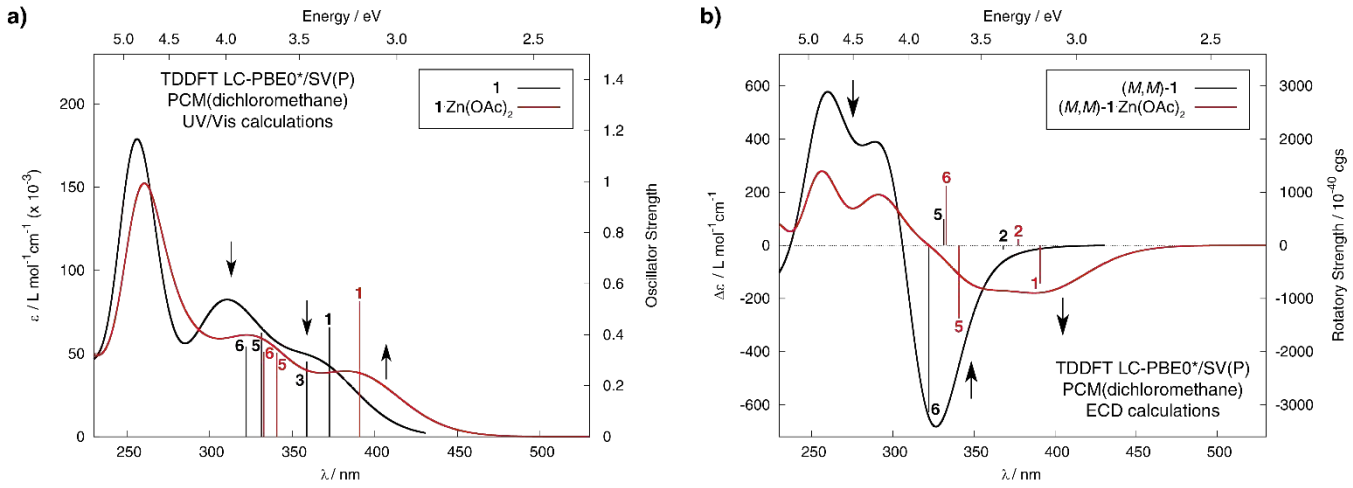

Figure 5. Comparison of the simulated UV/Vis (panel a) and ECD (panel b) spectra of the bis-helicenic bipyridine ligand **1** and of its corresponding Zn complex **1**·$Zn(OAc)_2$ (Boltzmann-averaged spectrum at 25 ºC based on the most populated conformers found). No spectral shift has been applied. Calculated excitation energies along with the corresponding oscillator and rotatory strengths (for the lowest-energy conformer in the case of **1**·$Zn(OAc)_2$) indicated as 'stick' spectra. Numbered excitations correspond to those analyzed in detail. See SI for a full set of data.

$Zn(OAc)_2 \cdot 2H_2O$ addition (see Figure 4b). For example, the strong positive ECD-active band at 273 nm decreases from +413 to +298 M^{-1} cm^{-1}, the strong negative band around 332 nm ($\Delta\varepsilon$ = -338 M^{-1} cm^{-1}) evolves into a new one centered at 342 nm ($\Delta\varepsilon$ = -202 M^{-1} cm^{-1}), and an additional negative band of medium intensity appears at 454 nm ($\Delta\varepsilon$ = -45 M^{-1} cm^{-1}). Furthermore, magnitude of the molar rotation significantly increases for **1**·$Zn(OAc)_2$ comparing to **1** (e.g. (*M*,*M*)-**1**·$Zn(OAc)_2$: $[\phi]_D^{23}$ = -25000° cm^2 $dmol^{-1}$, (*M*,*M*)-**1**: $[\phi]_D^{23}$ = -16700° cm^2 $dmol^{-1}$ (±5%, CH_2Cl_2, 1.9×10^{-4} M), see also SI). Finally, as presented in Figure 4c, Zn^{II} complexation led also to significant changes in the luminescence profile of **1**, with the appearance of a structureless intense fluorescence at 520 nm (ϕ = 44%) accompanied by a structured emission at 421 and 446 nm that resembles that from the ligand itself in line with the presence of equilibrium between **1** and **1**·$Zn(OAc)_2$. This was followed by a striking change in the emission colour from blue to green (see Figure 8d). Note that in order to obtain full transformation of the emission signal corresponding to full conversion to Zn complex, it was necessary to add an excess of $Zn(OAc)_2$. Finally, having in hands chiral species displaying efficient fluorescence, it was appealing to examine their corresponding circularly polarized luminescence (CPL).[22,23] The CPL responses for (*P*,*P*)-/(*M*,*M*)-**1** and (*P*,*P*)-/(*M*,*M*)-**1**·$Zn(OAc)_2$ were thus measured in CH_2Cl_2 at rt and the resulting spectra are depicted in Figure 6, showing maximum $g_{lum} = 2\Delta I/I$ values of -3.7 and +4.8 × 10^{-3} for (*M*,*M*)-**1** and (*P*,*P*)-**1** at 425 nm, respectively, and of -1.5 and +1.8 × 10^{-3} for (*M*,*M*)-**1**·$Zn(OAc)_2$ and (*P*,*P*)-**1**·$Zn(OAc)_2$ at 495 nm, respectively, which appear quite similar to values found for the previously examined helicene-bipyridine and bis-helicenic terpyridine systems (*i.e.* 3.4 × 10^{-3} and 7 × 10^{-3} for the bipyridine and terpyridine ligand, respectively, and 1 × 10^{-3} for the terpyridine Zn complex, *P* enantiomers).[10h,11] Accordingly, based on the fact that **1** and its Zn complex show clearly distinct and good CPL responses, one may envision to use CPL-activity at one chosen fixed wavelength to read-out the coordination/decoordination switching process for **1**.

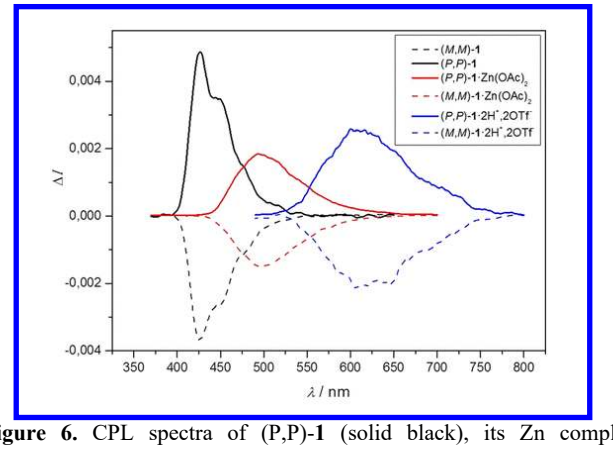

Figure 6. CPL spectra of (P,P)-**1** (solid black), its Zn complex (P,P)-**1**·$Zn(OAc)_2$ (solid red), and its fully protonated species (P,P)-**1**·$2H^+$, $2OTf^-$ along with the corresponding spectra of their mirror-images (dash lines) measured in CH_2Cl_2 at rt ($C \approx 1 \times 10^{-5}$ M). Excitation wavelengths: λ_{ex} at 350 nm for **1** and **1**·$Zn(OAc)_2$; 460 nm for **1**·$2H^+$, $2OTf^-$. Maximum intensities have been normalized to 2.

Calculations (TDDFT LC-PBE0*/SV(P) with a continuum solvent model for CH_2Cl_2) performed for bis-helicenic bipyridine complex of Zn^{II} correctly reproduce the spectral trends observed experimentally upon binding of the metal fragment to **1**. Due to a lack of X-ray crystal data for the **1**·$Zn(OAc)_2$ compound, various conformations, differing in the spatial arrangement of acetate ligands around Zn^{II}, were considered in geometry optimizations of this system. The lowest-energy structures with non-negligible populations, all comprising acetate ion(s) coordinated to the metal center in a bidentate fashion (see SI), reveal very similar overall UV/Vis and ECD spectral envelopes, and, as can be seen from Figure 5, their Boltzmann-averaged spectra agree well with the experiment. Contrary to the previously reported bis-helicenic terpyridine chiroptical switching system,[11] the simulated UV/Vis and ECD spectra of the ligand **1** in the *cis* conformation of the bipyridine fragment clearly differ from those calculated for **1**·$Zn(OAc)_2$ (see SI). This may indicate that the spectral modifications accompanying **1**→**1**·$Zn(OAc)_2$

transition originate predominantly from electronic rather than geometric changes occurring in **1** upon complexation. Indeed, although no contributions of Zn *d* orbitals to the helicenic π-electron system can be noticed, as expected for closed-shell d^{10} metal center, electronic interaction between Zn and **1** induces polarization of electron density and has a stabilizing effect on the orbital energies in **1**·$Zn(OAc)_2$ vs. **1** (see Figure 3 and SI) that may rationalize differences in the spectral envelopes of **1** and **1**·$Zn(OAc)_2$.[11,10h] In particular, a shift of the electronic density towards terminal rings of helicenes' moieties in HOMO and towards bipyridine fragment in LUMO, along with a decrease in the HOMO-LUMO gap due to a strong energetic stabilization of the LUMO level, observed for **1**·$Zn(OAc)_2$ as compared to **1**, activate intense low-energy helicene→bipyridine CT excitation within the ligand π-system (see excitation no. 1 calculated at ca. 390 nm of predominantly HOMO-LUMO character, Figure 5 and SI). The excitation is responsible for the appearance of the additional low-energy intensity in the UV/Vis and ECD spectra upon complexation. Furthermore, the calculations link the pronounced modification (a red-shift and a decrease in intensity) of the main band in the ECD spectrum for **1**·$Zn(OAc)_2$ vs. **1** to the presence of two excitations with strong rotatory strength values of opposite signs (nos. 5 and 6 calculated at ca. 340 and 330 nm, respectively) which involve mainly helicene→bipyridine CT transitions rather than classical helicene-centered π-π* ones (*vide supra*). The aforementioned activation of low-energy CT transitions in **1** due to Zn^{II} coordination rationalizes also the experimentally observed emission switching process which is quite well reproduced by the computations: from 409 nm S_1-S_0 fluorescence calculated for **1** to 440-470 nm (depending on the conformer) for **1**·$Zn(OAc)_2$. Note that strong interaction between Zn^{II} and **1** in **1**·$Zn(OAc)_2$ was indeed confirmed using the ETS-NOCV[24] charge and bonding-energy analysis, which showed one main NOCV-based contribution to the total deformation density corresponding to a formation of the Zn^{II}-N σ-bonding associated with a charge transfer from lone-pair (LP) of bipyridine nitrogen atoms to the metal center (Figure 3).

The reversibility of the Zn^{II} binding process was examined by using *N*,*N*,*N*',*N*'-tetrakis(2-pyridylmethyl)ethane-1,2-diamine (TPEN) as a competitive ligand. Indeed, upon addition of TPEN, the system returned to its original state, *i.e.* chiral (*P*,*P*)- and (*M*,*M*)-**1** non-coordinated species. Up to 9-10 steps could be performed upon successive additions of 1 equiv. of $Zn(OAc)_2$ and TPEN, following the ECD tuning at the selected wavelengths at which the changes are clearly visible (for example, 274 nm: $\Delta\Delta\varepsilon$ = 150 M^{-1} cm^{-1}, see Figure 4d). Accordingly, the bis-helicenic bipyridine system **1** constitutes another example of a chemically-triggered chiroptical switch with multi-output read-out including UV/Vis, ECD, and luminescence, for which the switching process is accompanied by nanomechanical molecular movements interconverting a *trans* conformation in the free ligand to a *cis* one in the Zn-complex.[11]

Having established that the Zn^{II} coordination/decoordination effectively and reversibly interconverts transoid and cisoid forms of **1**, the question arises as to whether **1** can act as a molecular hinge. Molecular hinges are systems that demonstrate a high relative amplitude of motion (> 90°) accompanied by controllable unidirectional 'open-close' movements. The first of these requirements can be in general easily fulfilled for 2,2'-bipyridine-based systems thanks to efficient metal-ion complexation / decomplexation processes that transform an 'open' non-complexed form (nitrogen atoms in *trans* configuration, NCC'N' dihedral angle of ~180°) to a 'closed' complexed one (nitrogen atoms in *cis* configuration, NCC'N' dihedral angle of ~0°) and vice versa. The second one (*i.e.* a control of the orientation of the movement between 'open' and 'close' states) is, however, more difficult to achieve as a rotation around the C-C' bipyridine bond is usually possible in both directions. The unidirectionality of the movement can be enforced for example by introducing a *meta*-bridge within the bipyridine part.[21a,b] However, one could envision a similar effect in systems with spatially extended substituents attached to the bipyridine core (such as for example helicenes' moieties in **1**) since such fragments, interacting with each other during a rotation around the C-C' axis, could make one of 'open'↔'closed' transition pathways preferable over the other providing a control over a movement' direction. Accordingly, the energy profile for the full rotation around the C-C' axis in **1** was calculated both at DFT and DFT-D3 (*i.e.* with inclusion of van der Waals (dispersive) forces via semi-empirical approach, see SI) level of theory and the corresponding results are shown in Figure 7. As can be seen, additional stabilizing dispersion interactions between helicenes' moieties located close to each other in the structure II (see also Figure S2.18 in the SI for overlays of the corresponding DFT- and DFT-D3-optimized geometries) lower its energy compared to the structure IV in which helicenes' fragments are located apart (compare 7.0 kcal/mol vs. 8.9 kcal/mol for II and IV, respectively, relative to the lowest-energy structure I). This leads to asymmetry of the rotational profile for **1**, which indicates that 'open': I → 'close': III transition may preferably occur via the pathway proceeding through structure II. However, even if we disregard a known tendency of DFT-D3 dispersion corrections to overestimate interactions between the aromatic rings of the helicene moieties,[25] this asymmetry seems to be too small to guarantee the preferential direction of rotation in **1**. Accordingly, it is rather unlikely that this type of systems can act as molecular 'hinges'.

Chiroptical switching activity of 1 induced via protonation/deprotonation process

Finally, the acid-base switching for **1** was studied by using *i*) triflic acid and *ii*) triethylamine for protonation and deprotonation step, respectively (see Scheme 1). Upon adding aliquots of triflic acid (0.2 equiv.) to (*M,M*)-**1** in CH_2Cl_2 until saturation at 8 equivs, a full protonation of (*M,M*)-**1** is expected with a formation of doubly protonated species (*M,M*)-**1**·$2H^+$, $2OTf^-$. The process was followed by UV/Vis, ECD, and emission measurements, and the corresponding responses are presented in Figure 8. As can be seen, the UV/Vis spectrum of the protonated species (*M,M*)-**1**·$2H^+$, $2OTf^-$ significantly differs from that of the non-protonated system (*M,M*)-**1** with 1) a slight increase in intensity of the band centered at 275 nm accompanied by its 5 nm bathochromic shift, 2) an intensity decrease of the bands at 325 and 383 nm, and 3) an appearance of strong broad band at longer wavelengths (420-550 nm, λ_{max} = 475 nm, ε = 15000 M^{-1} cm^{-1}, Figure 8a). Similarly, the ECD spectrum of (*M,M*)-**1** was substantially modified upon protonation showing a less intense positive band at 275 nm ($\Delta\varepsilon$ = +330 M^{-1} cm^{-1}), a less intense negative band at 335 nm ($\Delta\varepsilon$ = -243 M^{-1} cm^{-1}), and an additional moderate negative band at 460 nm ($\Delta\varepsilon$ = -32 M^{-1} cm^{-1}) for the (*M,M*)-**1**·$2H^+$, $2OTf^-$ enantiomer (Figure 8b). Significant changes can also be observed for the luminescence profile of **1** for which, upon

adding triflic acid, a structureless intense orange-red fluorescence emission appeared around 600 nm (ϕ = 28%), while the structured blue emission at 421 and 446 nm, coming from the non-protonated system itself (*vide supra*), almost completely disappeared (Figures 8c and 8d). This clearly confirms that under saturation conditions only protonated species are present in the solution. Finally, the CPL responses of (*M*,*M*)- and (*P*,*P*)-**1**·2H$^+$, 2OTf$^-$ were also measured in CH_2Cl_2 at rt (see Figure 6) and showed distinct signals centered around 605 nm with g_{lum} maxima of the same order of magnitude as found for **1** and **1**·Zn(OAc)$_2$, namely -2.0 and +2.5 × 10^{-3} for (*M*,*M*) and (*P*,*P*) enantiomer, respectively. Note that very similar g_{lum} values were also obtained for protonated species of helicenic bipyridine system, although introduction of two helicene moieties onto the bipyridine core leads to much more red-shifted CPL signal (compare 643 nm for **1** vs. 590 nm with g_{lum} = 3.2 × 10^{-3} (*P* enantiomer) for helicene-bipyridine).[10h] Summarizing, thanks to reversibility of the process (upon addition of aliquots of NEt_3 the UV/Vis and ECD, emission and CPL activity spectra of non-protonated species were recovered), the presented here bis-helicenic bipyridine system **1** can also act as an efficient pH-triggered (chir)optical switch.[26]

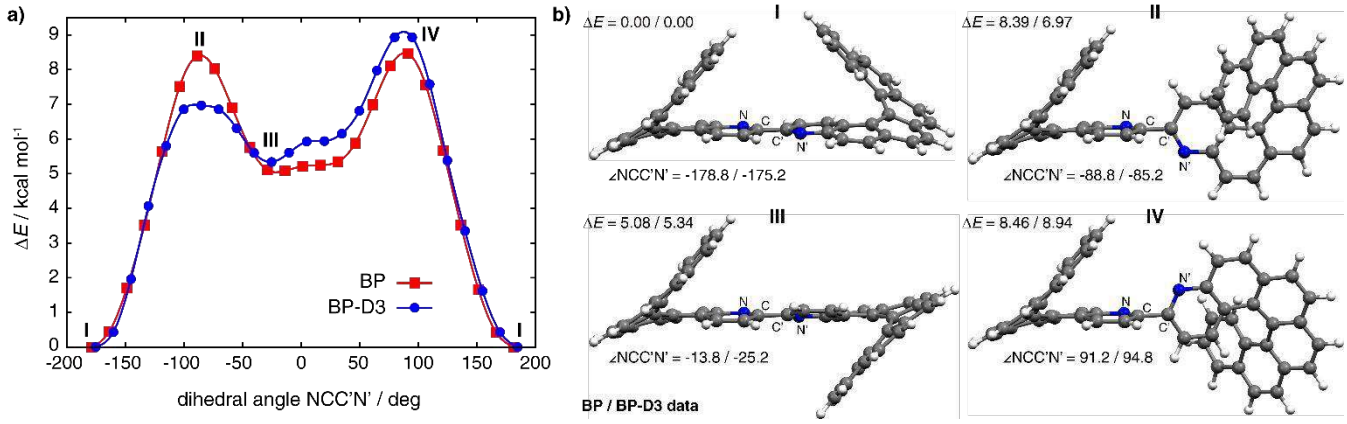

Figure 7. Energy profiles for the rotation around CC' bond in bis-helicenic bipyridine **1** (panel a) along with molecular structures corresponding to their characteristic points (panel b). BP and BP-D3 SV(P) calculations with continuum solvent model for CH_2Cl_2. Values listed in panel b are relative energies ΔE (in kcal/mol) and NCC'N' dihedral angles (in deg) obtained with BP / BP-D3.

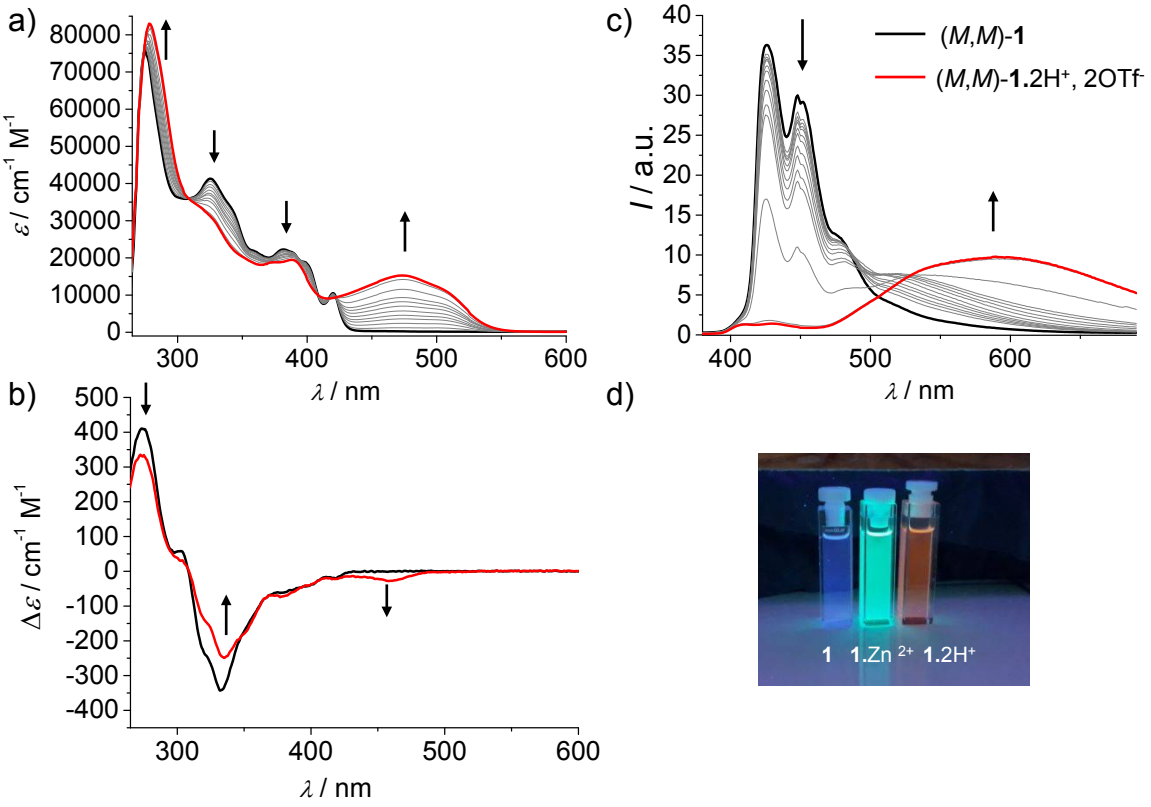

Figure 8. Evolution of UV/Vis spectrum (panel a), ECD spectrum (panel b), and fluorescence spectrum (panel c) of (*M*,*M*)-**1** upon addition of TfOH aliquots (0.2 equiv. until saturation at 8 equivs; *C* 2.2 × 10^{-5} M, CH_2Cl_2, rt, λ_{ex} = 350 nm). Panel d: Picture of emissive solutions of **1**, its Zn^{II} complex, and its protonated species irradiated with 365 nm lamp.

To provide some insight into experimentally observed tuning of photophysical and chiroptical properties in **1** upon its protonation, (TD)DFT calculations were then performed for both singly (n = 1) and doubly (n = 2) protonated **1**·nH$^+$ species, as they all are likely to be present in the reaction mixture below saturation limit. As expected,[27] the mono-protonated system preferentially adopts a conformation with nitrogen atoms within bipyridine core placed in *cis* configuration (see structure **1**·H$^+$-I in Figure S2.9 in the SI), while for di-protonated species transoid arrangement is favoured (**1**·2H$^+$-I and **1**·2H$^+$-II). Although the corresponding TDDFT calculations provide less satisfactory (than in the case of the neutral species) agreement with the experimental spectral envelopes for **1**·2H$^+$, 2OTf$^-$, as a low-energy band computed for **1**·2H$^+$ appears too red-shifted, which is likely due to solvent and counter-ion(s) effects,[10h,28] the most important changes in photophysical and chiroptical properties of **1** observed experimentally upon its protonation are reproduced correctly. In particular, in line with the experiment, the computations for the protonated species demonstrate *i*) appearance of additional absorption and ECD intensity above 420 nm, *ii*) a significantly reduced intensity of the ECD band around 330 nm, and *iii*) a large red-shift (> 100 nm) of the emission signal. All these features can be linked to a strong impact of protonation on the π-electronic system of **1** that manifests itself through a clear spatial separation of the frontier MOs of **1**·nH$^+$, with HOMO predominantly localized on the central and terminal parts of helicenic moieties and LUMO limited to the bipyridine core and the adjacent rings, accompanied by the strong stabilization of their energy levels (see Figure 3 and SI), especially pronounced for LUMO, resulting in a significant reduction of the HOMO-LUMO gap. Accordingly, photophysical and chiroptical properties of **1** upon its protonation appears to be dominated by low-energy CT-type transitions rather than classical helicene-centered π-π* ones (see SI).[10h] For example, the new lowest-energy UV/Vis and ECD bands in **1**·2H$^+$ correspond to a clear CT electronic transition between helicene π-system and bipyridine core of the predominant HOMO-LUMO composition that further amplifies its CT character. Decreased (increased) contributions from helicene-centered π-π* (CT-type) transitions to the excitations calculated in the medium-energy part of the ECD spectra are also responsible for a decrease in intensity of the ECD band around 330 nm. Similarly, very pronounced red-shift of the fluorescence signal for **1** observed upon protonation can be traced back to the predominant CT character of the corresponding S_1 excited state and the stabilization of the LUMO level. Note also that the calculations enable to shed some light on evolution of the emission spectra of **1** upon adding aliquots of triflic acid that involves *i*) a gradual diminishing of the signal centered at 420 and 440 nm accompanied by a gradual rise of emission intensity around 520 nm observed before reaching saturation, and *ii*) disappearance of the signal centered at 420 and 440 nm and appearance of separate intense band around 600 nm seen after saturation conditions are met. Based on the computed S_1-S_0 fluorescence for the neutral system **1** (409 nm, see SI) and for its protonated species **1**·nH$^+$ (495 nm for n = 1, and 660-690 nm (depending on the conformer) for n = 2), it appears therefore that below saturation limit neutral and mainly singly protonated species are present in the solution, while above it doubly protonated species clearly predominate.

CONCLUSIONS

In conclusion, a novel chiral 2,2'-bipyridine-based system endowed with two helicenic units has been synthesized in enantiopure forms from a 3-bromo-substituted 4-aza[6]helicene. This compound displays strong photophysical and chiroptical properties including intense UV/Vis, ECD and emission spectra, and good CPL activity. The 2,2'-bipyridine chelating ability and basic properties were studied through the coordination and protonation processes with $Zn(OAc)_2$ and triflic acid, respectively. These reversible processes, as shown by quantum-chemical calculations, activate tuning between π-π*-type and charge-transfer-type excitations that leads to efficient changes of the spectral properties of **1**. Accordingly, a new example of versatile molecular chiroptical switch emerges, behaving like a chiral dye. Finally, the **1** / **1**·2H$^+$, 2OTf switching system emits a circularly polarized luminescence in the red region, which may be of interest in the field of bioimaging.

EXPERIMENTAL SECTION

All experiments were performed under an atmosphere of dry argon using standard Schlenk techniques. Commercially available reagents were used as received without further purification. All solvents were dried according to standard procedures. Preparative separations were carried out by gravity column chromatography over silica gel (Merck Geduran 60, 0.063-0.200 mm) in 3.5-20 cm columns. Analytical thin layer chromatographies (TLC) were performed using aluminium-coated Merck Kieselgel 60 F254 plates. NMR spectra were recorded on a Bruker 300 Avance (^{1}H: 300 MHz; ^{13}C: 75 MHz), a Bruker Avance 400 or a Bruker Avance 500 (^{1}H: 500 MHz; ^{13}C: 125 MHz) spectrometers at rt, unless stated otherwise, using partially deuterated solvents as internal standards. Coupling constants (J) are given in Hz and chemical shifts (δ) in ppm. Multiplicities are denoted as follows: s = singlet, d = doublet, t = triplet, m = multiplet, while b = broad. Assignment of hydrogen atoms is based on 1H-1H COSY experiment. Assignment of carbon atoms is based on HMBC, HMQC and DEPT-135 experiments. Mass spectrometry was performed by the CRMPO, University of Rennes 1. Specific rotations ($[\alpha]_D^{20}$ in deg cm^2 g^{-1}) were measured in a 1 dm thermostated quartz cell on a PerkinElmer Model 341 polarimeter. Molar rotations $[\phi]_D^{20}$ are given in deg cm^2 dmol^{-1}. Circular dichroism (in M^{-1} cm^{-1}) was measured on a Jasco J-815 Circular Dichroism Spectrometer (IFR140 facility - Biosit - University of Rennes 1). For details on UV/Vis and non-polarised luminescence measurements see SI. Photoirradiation experiments were performed on a Heraeus TQ718 immersion Hg lamp (150 W).

3-Bromo-4-aza[6]helicene 5. Helicene derivative **5** was prepared in two steps, *i.e.* by a Wittig reaction followed by a photocyclization. 1) First, benzo[g]phenanthren-3-ylmethyl triphenylphosphonium bromide **2** was prepared according to the literature.[16] A solution of **2** (400 mg, 0.686 mmol) in dry THF (16 mL) was cooled to -78º C and then n-BuLi (0.34

mL, 2.2 M in hexanes, 0.748 mmol) was added dropwise. The suspension turned orange and was left to stir at -78º C for 20 minutes, then the reaction mixture was warmed up to room temperature and kept stirring for 20 minutes more before cooling again (dark-red color). A solution of 6-bromo-2-pyridinecarboxaldehyde **3** (116 mg, 0.624 mmol) in dry THF (5 mL) was added at -78º C. The reaction mixture was warmed up to room temperature and stirred for 5 hours. The orange suspension was filtered over Celite® and washed with THF. The solvent was stripped off and the olefin **4** was obtained as an *E* and *Z* isomers (230 mg, 90 %) which was used as such in the next step. 2) In a flask well-adapted to the immersion Hg lamp, a solution of the olefinic precursor **4** (100 mg, 0.243 mmol) in degassed toluene (700 mL) was prepared. Iodine (123 mg, 0.486 mmol) and propylene oxide (0.85 mL, 12 mmol) were then added. The solution was strongly stirred overnight for 15 hours under the 150 W Hg lamp. The crude mixture was evaporated under vacuum and the product was purified by column chromatography (SiO_2, heptane:Et_3N 0.5% for packing, and the heptane:ethyl acetate 5-15%). The reaction was repeated five times (500 mg of precursor) to prepare (±)-**5** as a yellow solid (222 mg, 45%).

Enantiopure *M*- and *P*-**5** samples were obtained by HPLC separation over a chiral stationary phase (see SI).

^{1}H NMR (300 MHz, CD_2Cl_2) δ: 6.67 (1H, d, J = 9.0 Hz), 6.81 (1H, bt, J = 7.6 Hz), 7.32 (1H, bt, J = 7.6 Hz), 7.54 (1H, d, J = 8.6 Hz), 7.67 (1H, d, J = 9.0 Hz), 7.89 (1H, bd, J = 8.0 Hz), 7.96 (2H, bs), 8.00-8.11 (5H, m), 8.22 (1H, d, J = 9.0 Hz) ppm. ^{13}C{1H} NMR (75 MHz, CD_2Cl_2) δ: 123.8, 124.2, 124.9, 126.0, 126.6, 126.7, 127.65, 127.7, 127.8, 127.8, 128.2, 128.5, 128.6, 128.9, 129.7, 131.7, 131.9, 132.3, 132.8, 134.0, 137.8, 140.8, 148.3 ppm. HR-MS (QTOF), ESI, *m/z*: calcd. for $C_{25}H_{15}N^{79}Br$ $[M+H]^+$: 408.0382; found: 408.0383. Mp = 165-169 °C.

3,3'-Bis-4-aza[6]helicene 1. Helicene derivative **1** was synthesized by means of a Negishi coupling of the enantiopure 3-bromo-4-aza[6]helicene **5**. To a solution of *n*-BuLi (100 µL, 0.168 mmol) in dry THF (0.4 mL) at -78º C, a solution of 3-bromo-4-aza[6]helicene **5** (36 mg, 0.088 mmol) in dry THF (0,4 mL) was added dropwise. A color of reaction mixture changed from colorless to wine red at the end of the addition. The solution was kept stirring for 30 minutes at -78º C and then $ZnCl_2$ (225 µL, 1.0 M in diethyl ether) was added. The mixture changed from a red-wine solution to a dark-yellow suspension. The temperature was warmed up to 0º C for 1 hour and then to room temperature for 2 hours more. The reaction mixture was cooled again to 0º C and the 3-bromo-4-aza[6]helicene **5** (33 mg, 0.080 mmol) and catalyst $Pd(PPh_3)_4$ (3 mg) were then added in solution in dry THF (0.3 mL). After 1 hour at 0º C, the reaction mixture was warmed up to reflux. After stirring and refluxing for 15 hours, a bright-yellow precipitate was obtained. Dichloromethane (15 mL) and TPEN (36 mg, 0.0849 mmol) were then added and the mixture sonicated for 5 minutes. Final purification by column chromatography (SiO_2, heptane:ethyl acetate 15%) yielded **1** (30 mg, 57%) as a bright-yellow solid. Note that around 10% of 4-aza[6]helicene was obtained as a side product.

The same procedure was used to prepare enantiopure (*M*,*M*)- and (*P*,*P*)-**1** by starting from *M*- or *P*-**5**, respectively. The *meso*-**1** compound was not characterized due to low solubility and small mass quantity available.

(*M*,*M*)-**1**: ^{1}H NMR (400 MHz, CD_2Cl_2) δ: 6.86 (2H, t, J = 7.6 Hz, H_{15}), 7.37 (2H, t, J = 7.6 Hz, H_{14}), 7.73 (2H, d, J = 8.5 Hz), 7.98 (2H, d, J = 7.9 Hz), 8.02 (8H, dd, J = 9.0, 3.0 Hz), 8.05-8.08 (7H, m), 8.08-8.16 (3H, m), 8.20 (2H, d, J = 8.9 Hz) ppm.. ^{13}C{1H} NMR (400 MHz, CD_2Cl_2) δ: 154.7, 147.7, 136.1, 133.9, 132.8, 132.3, 132.0, 130.9, 130.2, 130.0, 128.9, 128.6, 128.3, 127.8, 127.6, 126.8, 126.4, 126.1, 126.0, 124.5, 117.4 ppm. HR-MS (QTOF), ESI, *m/z*: calcd. for $C_{50}H_{28}N_2Na$ $[M+Na]^+$ 679.2145 found (pos.) 679.2146. Mp = 170-175 °C.

1·Zn(OAc)$_2$ complex. The complexation was carried out by simple solvation of the ligand **1** (5 mg, 7.6 mmol) and $Zn(OAc)_2{\cdot}2H_2O$ (1.8 mg, 8.4 mmol, 1.1 equivalents) in 5 mL of dichloromethane. One minute of ultrasounds bath was used for total solvation of the complex. The colour intensity increased upon complexation, and once evaporated the solvent, only one set of signals was visible in ^{1}H NMR spectra.

The same procedure was used to prepare enantiopure (*M*,*M*)- and (*P*,*P*)-**1**·$Zn(OAc)_2$ by starting from (*M*,*M*)- or (*P*,*P*)-**1**, respectively.

(*M*,*M*)-**1**·$Zn(OAc)_2$: ^{1}H NMR (400 MHz, CD_2Cl_2) δ: 2.07 – 2.00 (6H, s), 6.72 (2H, t, J = 7.6 Hz, H_{15}), 7.10 (2H, t, J = 7.6 Hz, H_{14}), 7.28 (2H, d, J = 9.0 Hz), 7.58 (2H, d, J = 8.5 Hz, H_{16}), 7.79 (2H, d, J = 8.0 Hz, H_{13}), 7.91-8.02 (4H, m), 8.11 (4H, bs), 8.14 (2H, d, J = 8.1 Hz), 8.24 (2H, d, J = 8.1 Hz), 8.34 (2H, d, J = 9.0 Hz) 8.52 (2H, d, J = 9.0 Hz), 8.68 (2H, d, J = 9.0 Hz) ppm. ^{13}C: After experiment overnight in 500 MHz the signals were not large enough to give an accurate set of peaks. Yellowish solid; Mp = 162-167 °C.

Acid-base switching of (*M*,*M*)-1. To a solution of (*M*,*M*)-**1** (2.2×10^{-5} M in CH_2Cl_2) were added aliquots of a solution of CF_3SO_3H (1.14×10^{-3} M in CH_2Cl_2) until saturation of the UV/Vis and ECD signals (5 µL added). Upon addition of aliquots of NEt_3 (1.4×10^{-3} M in CH_2Cl_2), the UV/Vis and ECD spectra of (*M*,*M*)-**1** were recovered.

ASSOCIATED CONTENT

Supporting Information

^{1}H, ^{13}C, and COSY spectra of compounds **5**, (*M*,*M*)-**1**, and (*M*,*M*)-**1**·$Zn(OAc)_2$. X-ray diffraction data of **1** and **5**. HPLC conditions for **1** and **5**. Photophysical and chiroptical properties of (*M*,*M*)-**1**, (*M*,*M*)-**1**·$Zn(OAc)_2$, and (*M*,*M*)-**1**·$2H^+$, $2OTf^-$. Computational details. Additional calculated results. This material is available free of charge on the ACS Publications website at DOI:

AUTHOR INFORMATION

Corresponding Authors

* jeanne.crassous@univ-rennes1.fr

* srebro@chemia.uj.edu.pl

ORCID

Jeanne Crassous: 0000-0002-4037-6067X

Monika Srebro-Hooper: 0000-0003-4211-325X

Notes

The authors declare no competing financial interest.

ACKNOWLEDGMENTS

We acknowledge the Ministère de l'Education Nationale, de la Recherche et de la Technologie, the Centre National de la Recherche Scientifique (CNRS), the CNRS (Chirafun network), and the ANR (12-BS07-0004-METALHEL-01), for financial support. H. I. thanks the Région Bretagne for financial support. K. D. thanks The University of Gabès, the University of Rennes 1 and Campus France for financial support. M.S.-H. acknowledges the young researchers' T-subsidy from the Ministry of Science and Higher Education in Poland.

REFERENCES

(1) a) Amabilino, D. B. Chiral nanoscale systems: preparation, structure, properties and function. *Chem. Soc. Rev.* **2009**, *38*, 669-670; b) Amabilino, D. B. *Chirality at the Nanoscale. Nanoparticles, Surfaces, Materials and more*, Wiley-VCH: **2009**.

(2) a) Feringa, B. L. The Art of Building Small: From Molecular Switches to Molecular Motors. *J. Org. Chem.* **2007**, *72*, 6635-6652; b) Canary, J. W. Redox-triggered chiroptical molecular switches. *Chem. Soc. Rev.* **2009**, *38*, 747-756; c) Browne, W. R.; Feringa, B. L. *Molecular Switches*, Wiley-VCH, Weinheim, **2011**, chapter 5, pp 121-180.

(3) Balzani, V.; Credi, A.; Venturi, M. *Molecular Devices and Machines. Concepts and Perspectives for the Nanoworld*, Wiley-VCH, Weinheim, **2008**.

(4) a) You, L.; Zha, D.; Anslyn, E. V. Recent Advances in Supramolecular Analytical Chemistry Using Optical Sensing. *Chem. Rev.* **2015**, *115*, 7840-7892; b) Canary, J. W.; Mortezaei, S.; Liang, J. Transition metal-based chiroptical switches for nanoscale electronics and sensors. *Coord. Chem. Rev.* **2010**, *254*, 2249-2266.

(5) a) Zhao, D.; Neubauer, T. M.; Feringa, B. L. Dynamic control of chirality in phosphine ligands for enantioselective catalysis. *Nature Comm.* **2015**, *6*, 6652; see also reviews: b) Vlatkovic, M.; Collins, B. S. L.; Feringa, B. L. Dynamic Responsive Systems for Catalytic Function. *Chem. Eur. J.* **2016**, *22*, 17080-17111; c) Dai, Z.; Lee, J.; Zhang, W. Chiroptical switches: Applications in sensing and catalysis. *Molecules* **2012**, *17*, 1247-1277.

(6) a) Chen, C.-F.; Shen, Y. *Helicene Chemistry - From Synthesis to Applications*, Springer, **2017**; b) Rajca, A. Miyasaka, M. In *Functional Organic Materials*, Wiley-VCH, **2007**, pp 547-581; c) Shen, Y.; Chen, C.-F. Helicenes: Synthesis and Applications. *Chem. Rev.* **2011**, *112*, 1463-1535; d) Gingras, M. One hundred years of helicene chemistry. Part 3: applications and properties of carbohelicenes. *Chem. Soc. Rev.* **2013**, *42*, 1051-1095; e) Saleh, N.; Shen, C.; Crassous, J. Helicene-based transition metal complexes: synthesis, properties and applications. *Chem. Sci.* **2014**, *5*, 3680-3694; f) Isla, H.; Crassous, J. Helicene-based chiroptical switches. *C. R. Chimie* **2016**, *19*, 39-49.

(7) Berova, N.; Polavarapu, P. L.; Nakanishi, K.; Woody R. W. (Eds.), *Comprehensive Chiroptical Spectroscopy*, John Wiley & Sons, **2012**, vol. 1&2.

(8) a) Lehn, J.-M. *Supramolecular Chemistry: Concepts and Perspectives*. VCH: Weinheim, **1995**; b) Sauvage, J.-P. *Perspectives in Supramolecular Chemistry: Transition Metals in Supramolecular Chemistry*, John Wiley & Sons, **1999**; c) Elschenbroich, C. *Organometallics*. Wiley-VCH: Weinheim, **2006**.

(9) a) Brunner, H. Optically Active Organometallic Compounds of Transition Elements with Chiral Metal Atoms. *Angew. Chem. Int. Ed.* **1999**, *38*, 1194-1208; b) Knof, U.; von Zelewsky, A. Predetermined Chirality at Metal Centers. *Angew. Chem. Int. Ed.* **1999,** *38*, 302-322; c) Amouri, H.; Gruselle, M. *Chirality in Transition Metal Chemistry: Molecules, Supramolecular Assemblies and Materials*. Wiley: Chichester, **2007**; d) Crassous, J. Chiral transfer in coordination chemistry. *Chem. Soc. Rev.* **2009**, *38*, 830-845; e) Crassous, J. Transfer of chirality to metal centers: recent advances. *Chem. Comm.* **2012**, ***48,*** 9684-9692; f) Miyake, H.; Tsukube, H. Coordination chemistry strategies for dynamic helicates: time-programmable chirality switching with labile and inert metal helicates. *Chem. Soc. Rev.* **2012**, *41*, 6977- 6991.

(10) a) Anger, E.; Srebro, M.; Vanthuyne, N.; Toupet, L.; Rigaut, S.; Roussel, C.; Autschbach, J.; Crassous, J.; Réau, R. Ruthenium-vinylhelicenes: remote metal-based tuning and redox switching of the chiroptical properties of a helicene core. *J. Am. Chem. Soc.* **2012**, *134*, 15628-15631; b) Srebro, M.; Anger, E.; Moore, II, B.; Vanthuyne, N.; Roussel, C.; Réau, R.; Autschbach, J.; Crassous, J. Ruthenium-grafted vinylhelicenes: chiroptical properties and redox switching. *Chem. Eur. J.* **2015**, *21*, 17100-17115; c) Shen, C.; Loas, G.; Srebro-Hooper, M.; Vanthuyne, N.; Toupet, L.; Cador, O.; Paul, F.; López Navarrete, J. T.; Ramírez, F. J.; Nieto-Ortega, B.; Casado, J.; Autschbach, J.; Vallet, M.; Crassous, J. Iron-alkynyl-helicenes: redox-triggered chiroptical tuning in the vibrational and telecommunication domain. *Angew. Chem. Int. Ed.* **2016**, *55*, 8062-8066; d) Saleh, N.; Vanthuyne, N.; Bonvoisin, J.; Autschbach, J.; Srebro-Hooper, M.; Crassous, J. Redox-triggered chiroptical switching activity of ruthenium(III)-bis-(β-diketonato) complexes bearing a bipyridine-helicene ligand. *Chirality* **2018**, *30*, 592-601; e) Shen, C.; Srebro-Hooper, M.; Weymuth, T.; Krausbeck, F.; López Navarrete, J. T.; Ramírez, F. J.; Nieto-Ortega, B.; Casado, J.; Reiher, M.; Autschbach, J.; Crassous, J. Redox-active Chiroptical Switching in Mono- and Bis-Iron-Ethynyl-Carbo[6]Helicenes Studied by Electronic and Vibrational Circular Dichroism and Resonance Raman Optical Activity. *Chem. Eur. J.* **2018**, *24*, 15067-15079; f) Shen, C.; He, X.; Toupet, L.; Norel, L.; Rigaut, S.; Crassous, J. Dual redox and optical control of chiroptical activity in photochromic dithienylethenes decorated with hexahelicene and bis-ethynyl-ruthenium units. *Organometallics* **2018**, 37, 697-705; g) Anger, E.; Srebro, M.; Vanthuyne, N.; Roussel, C.; Toupet, L.; Autschbach, J.; Réau, R.; Crassous, J. Helicene-grafted vinyl- and carbene-osmium complexes: an example of acid-base chiroptical switching. *Chem. Comm.* **2014**, *50*, 2854-2856; h) Saleh, N.; Moore, II, B.; Srebro, M.; Vanthuyne, N.; Toupet, L.; Williams, J. A. G.; Roussel, C.; Deol, K. K.; Muller, G.; Autschbach, J.; Crassous, J. Acid-base triggered switching of circularly polarized luminescence and electronic circular dichroism in organic and organometallic helicenes. *Chem. Eur. J.* **2015**, *21*, 1673-1681.

(11) Isla, H.; Srebro-Hooper, M.; Jean, M.; Vanthuyne, N.; Roisnel, T.; Lunkley, J. L.; Muller, G.; Williams, J. A. G.; Autschbach, J.; Crassous, J. Conformational changes and chiroptical switching of enantiopure bis-helicenic terpyridine upon Zn^{2+} binding. *Chem. Comm.* **2016**, ***52***, 5932-5935.

(12) Sato, K.; Harai. S. In *Cyclophane chemistry fot the 21st century*, H. Takamura (Ed.), Gayathri, A. **2002**, pp 173-198; b) Dumitrascu, F.; Dumitrescu, D. G.; Aron, I. Azahelicenes and other similar tri and tetracyclic helical molecules. *Arkivoc* **2010**, *1*, 1-10.

(13) Kaes, C.; Katz, A.; Hosseini, M. W. Bipyridine: The Most Widely Used Ligand. A Review of Molecules Comprising at Least Two 2,2'-Bipyridine Units. *Chem. Rev.* **2000**, *100*, 3553-3590.

(14) a) Fox, J. M.; Katz, T. J. Conversion of a [6]Helicene into an [8]Helicene and a Helical 1,10-Phenanthroline Ligand. *J. Org. Chem.* **1999**, *64*, 302-305; b) Deshayes, K.; Broene, R. D.; Chao, I.; Knobler, C. B.; Diederich, F. Synthesis of the helicopodands: novel shapes for chiral clefts. *J. Org. Chem.* **1991**, *56*, 6787-6795; c) Takenaka, N.; Sarangthem, R. S.; Captain, B. Helical Chiral Pyridine N-Oxides: A New Family of Asymmetric Catalysts. *Angew. Chem. Int. Ed.* **2008**, *47*, 9708-9710; d) Chen, J.; Captain, B.; Takenaka, N. Helical Chiral 2,2′-Bipyridine N-Monoxides as Catalysts in the Enantioselective Propargylation of Aldehydes with Allenyltrichlorosilane. *Org. Lett.* **2011**, *13*, 1654-1657; e) Saleh, N.; Srebro, M.; Reynaldo, T.; Vanthuyne, N.; Toupet, L.; Chang, V. Y.; Muller, G.; Williams, J. A. G.; Roussel, C.; Autschbach, J.; Crassous, J. Enantio-enriched CPL-active helicene-bipyridine-rhenium complexes. *Chem. Comm.* **2015**, ***51***, 3754-3757; f) Klívar, J.; Šámal, M.; Jančařík, A.; Vacek, J.; Bednárová, L.; Buděšínský, M.; Fiedler, P.; Starý, I.; Stará, I. G. Asymmetric Synthesis of Diastereo- and Enantiopure Bioxahelicene 2,2′-Bipyridines, *Eur. J. Org. Chem.* **2018**, *2018*, 5164-5178.

(15) Negishi, E. Magical Power of Transition Metals: Past, Present, and Future (Nobel Lecture). *Angew. Chem. Int. Ed.* **2011**, *50*, 6738-6764.

(16) Lightner, D. A.; Hefelfinger, D. T.; Powers, T. W.; Frank, G. W.; Trueblood, K. N. Hexahelicene. Absolute configuration. *J. Am. Chem. Soc.* **1972**, *94*, 3492-3497.

(17) (*P*,P**)-**1** means the racemic mixture of (*P*,*P*)- and (*M*,*M*)-**1**.

(18) Solovyov, K. N.; Borisevich, E. A. Intramolecular heavy-atom effect in the photophysics of organic molecules. *Phys.-Usp.*, **2005**, *48*, 231-253.

(19) a) Autschbach, J. Computing chiroptical properties with first-principles theoretical methods: background and illustrative examples. *Chirality* **2009**, *21*, E116-E152; b) Srebro-Hooper, M.; Autschbach, J. Calculating Natural Optical Activity of Molecules from First Principles. *Annu. Rev. Phys. Chem.* **2017**, *68*, 399-420.

(20) a) Rebek, Jr., J.; Trend, J. E.; Wattley, R. V.; Chakravorti, S. Allosteric effects in organic chemistry. Site-specific binding. *J. Am. Chem. Soc.* **1979**, *101*, 4333-4337; b) Rebek, Jr., J.; Wattley, R. V. Allosteric effects. Remote control of ion transport selectivity. *J. Am. Chem. Soc.* **1980**, *102*, 4853-4854; c) Rebek, Jr., J.; Costello, T.; Marshall, L.; Wattley, R.; Gadwood, R. C.; Onant, K. Allosteric effects in organic chemistry: binding cooperativity in a model for subunit interactions. *J. Am. Chem. Soc.* **1985**, *107*, 7481-7487.

(21) a) Bell, T. W.; Jousselin, H. Self-Assembly of a Double-Helical Complex of Sodium, *Nature* **1994**, *367*, 441-444; b) Haberhauer, G. Control of Planar Chirality: The Construction of a Copper-Ion-Controlled Chiral Molecular Hinge. *Angew. Chem. Int. Ed.* **2008**, *47*, 3635-3638; c) Ernst, S.; Haberhauer, G. A Unidirectional Open-Close Mechanism of

Metal-Ion-Driven Molecular Hinges with Adjustable Amplitude. *Chem. Eur. J.* **2009**, *15*, 13406-13416; d) Suzuki, Y.; Nakamura, T.; Iida, H.; Ousaka, N.; Yashima, E. Allosteric Regulation of Unidirectional Spring-like Motion of Double-Stranded Helicates. *J. Am. Chem. Soc.* **2016**, *138*, 4852-4859.

(22) a) Maeda H.; Bando, Y. Recent progress in research on stimuli-responsive circularly polarized luminescence based on π-conjugated molecules. *Pure Appl. Chem.*, **2013**, *85*, 1967-1978; b) Kumar, J.; Nakashima T.; Kawai, T. Circularly Polarized Luminescence in Chiral Molecules and Supramolecular Assemblies.*J. Phys. Chem. Lett.*, **2015**, *6*, 3445-3452; c) Sánchez-Carnerero, E. M.; Agarrabeitia, A. R.; Moreno, F.; Maroto, B. L.; Muller, G.; Ortiz M. J.; de la Moya, S. Circularly Polarized Luminescence from Simple Organic Molecules. *Chem. Eur. J.*, **2015**, *21*, 13488-13500.

(23) Examples of CPL-active oligomeric or discrete Zn complexes: a) Aoki, R.; Toyoda, R.; Kögel, J. F.; Sakamoto, R.; Kumar, J.; Kitagawa, Y.; Harano, K.; Kawai, T.; Nishihara, H. Bis(dipyrrinato)zinc(II) Complex Chiroptical Wires: Exfoliation into Single Strands and Intensification of Circularly Polarized Luminescence. *J. Am. Chem. Soc.* **2017**, *139*, 16024-16027; b) Imai, Y.; Nakano, Y.; Kawai, T.; Yuasa, J. A Smart Sensing Method for Object Identification Using Circularly Polarized Luminescence from Coordination-Driven Self-Assembly. *Angew. Chem. Int. Ed.* **2018**, *57*, 8973-8978; c) Reiné, P.; Ortuño, A. M.; Resa, S.; Alvarez de Cienfuegos, L.; Blanco, V.; Ruedas-Rama, M. J.; Mazzeo, G.; Abbate, S.; Lucotti, A.; Tommasini, M.; Guisán-Ceinos, S.; Ribagorda, M.; Campaña, A. G.; Mota, A.; G. Longhi, Miguel, D.; Cuerva, J. M. OFF/ON Switching of Circularly Polarized Luminescence by Oxophilic Interaction of Homochiral Sulfoxide-Containing *o*-OPEs with Metal Cations, *Chem. Commun*. **2018**, *54*, 13985-13988.

(24) Mitoraj, M. P.; Michalak, A.; Ziegler, T. A Combined Charge and Energy Decomposition Scheme for Bond Analysis. *J. Chem. Theory Comput*. **2009**, *5*, 962-975.

(25) a) Srebro, M.; Autschbach, J. Tuned range-separated time-dependent density functional theory applied to optical rotation. *J. Chem. Theory Comput*. **2012**, *8*, 245-256; b) El Sayed Moussa, M.; Srebro, M.; Anger, E.; Vanthuyne, N.; Roussel, C.; Lescop, C.; Autschbach, J.; Crassous, J. Chiroptical properties of carbo[6]helicene derivatives bearing extended π-conjugated cyano substituents. *Chirality* **2013**, *25*, 455-465; c) Friese, D. H.; Hättig, C. Optical rotation calculations on large molecules using the approximate coupled cluster model CC2 and the resolution-of-the-identity approximation. *Phys. Chem. Chem. Phys*. **2014**, *16*, 5942-5951.

(26) For a recent example of acid-base triggered CPL switch see: Takaishi, K.; Yasui, M.; Ema, T. Binaphthyl–Bipyridyl Cyclic Dyads as a Chiroptical Switch, *J. Am. Chem. Soc.* **2018**, *140*, 5334-5338.

(27) Alkorta, I.; Elguero, J.; Roussel, C. A theoretical study of the conformation, basicity and NMR properties of 2,2′-, 3,3′- and 4,4′-bipyridines and their conjugated acids. *Comput. Theor. Chem*. **2011**, *966*, 334-339.

(28) Nakai, Y.; Mori, T.; Sato, K.; Inoue, Y. Theoretical and Experimental Studies of Circular Dichroism of Mono- and Diazonia[6]helicenes. *J. Phys. Chem. A* **2013**, *117*, 5082-5092.